A rapid boundary perturbation algorithm for scattering by families of rough surfaces

David P. Nicholls *

Department of Mathematics, Statistics, and Computer Science, University of Illinois at Chicago, 851 South Morgan Street (MC 249), Chicago, IL 60607, United States

ARTICLE INFO

ABSTRACT

In this paper we describe a novel algorithm for the computation of scattering returns by families of rough surfaces. This algorithm makes explicit use of the fact that some scattering profiles of engineering interest (e.g., traveling ocean waves) come in branches parameterized analytically by a bifurcation quantity. Our approach delivers recursions which not only can be implemented to yield a rapid, robust and high-order numerical scheme, but also give a new proof of analyticity of scattering quantities with respect to the bifurcation parameter of the surface family. The real advantage of this new approach is that it computes, in one step, the scattered field for *all* possible members of the family of surfaces. By contrast, other state-of-the-art schemes must restart when the returns from a new surface are desired, so that the cost of our new approach is greatly advantaged when the number of samples of the family reaches even modest values. Numerical results which verify the accuracy of our approach and demonstrate their utility in computing grating efficiencies scattered by traveling surface ocean waves are presented.

© 2009 Elsevier Inc. All rights reserved.

1. Introduction

The interaction of acoustic or electromagnetic radiation with irregular obstacles plays a crucial role in a wide range of engineering applications including, e.g., remote sensing, radar imaging, and non-destructive testing. In this paper we focus upon the development of efficient numerical algorithms to simulate the scattering of two-dimensional linear acoustic waves from a *family* of impenetrable rough surfaces parameterized by a quantity, ε, meant to indicate the surface's height or slope. In particular, we exhibit a novel scheme which uses the parameterized nature of the scatterers in a fundamental way to produce solutions at a fraction of the cost of state-of-the-art solvers for even a mild sampling of the family.

An important example of a parameterized set of rough surfaces are the traveling wave solutions of the "water wave problem," which models the free-surface evolution of a large body of water (e.g., a lake or ocean). The study of the possible shapes and oceanographic properties of traveling wave solutions of the water wave problem [1,2] has a long history dating from the early contributions of Stokes [3], to the existence theories of Levi-Civita [4] and Struik [5], to the recent computations of the author and Reitich [6] (please see the excellent survey articles of Dias and Kharif [7] and Groves [8] for a comprehensive list of contributions). Of course, given a *fixed* ocean profile there are a wide variety of reliable algorithms to approximate the scattering of acoustic waves by a rough surface. However, none of these algorithms takes advantage of the special structure of the traveling waves: They come in bifurcation *families* [9,10] where only certain heights, slopes, and shapes are permitted. Importantly, the dependence of the fluid surface upon the bifurcation parameter, ε, is *analytic* so that it can be expressed as a *strongly convergent* power series. We use this latter fact to compute a power series representation of the scattered field

* Tel.: +1 312 413 1641; fax: +1 312 996 1491.
  E-mail address: nicholls@math.uic.edu

generated by *all* possible traveling waves of a given ocean depth and periodicity. With this, we have Taylor series representations of all near-field (e.g., surface velocity), far-field (e.g., efficiencies), and volumetric quantities of engineering interest, and thus we can produce any of these with negligible additional cost for a particular waveform. By contrast, current state-of-the-art methods must begin anew for every different ocean surface of interest so that, regardless of the efficiency of the method, its cost quickly swamps that of our new approach once a modest subset of waves is considered.

An added advantage of our method is that it enables a proof of the analyticity of a wide variety of scattering quantities (e.g., the scattered field) as a function of the traveling water wave bifurcation parameter, ε. Once our recursions are derived, this analyticity theorem is readily established using quite standard techniques. That these results can be derived from the very recursions that we implement numerically, indicates the very stable and robust behavior of our method which has been noted in this entire class of "Transformed Field Expansion" Boundary Perturbation methods [11,12,6].

The rest of the paper is organized as follows: In Section 2 we recall the governing equations of scattering of two-dimensional acoustic radiation by an impenetrable irregular surface. In Section 3 we discuss several popular numerical methods for the numerical simulation of these grating problems: integral equations (Section 3.1), field expansions (Sections 3.2 and 3.4), and our new transformed field expansions for families of gratings (Sections 3.5 and 3.6). We also discuss the particular family of surfaces we have in mind, the traveling water waves (Section 3.3); in Section 3.7 we give the outline of a proof of analyticity of the scattered field as a function of ε. We present numerical results in Section 4 featuring both verification of our algorithm (Section 4.1) and plots of efficiencies as one moves through the set of permissible traveling water waves (Section 4.2). Concluding remarks are given in Section 5.

2. Governing equations

Suppose that a time-harmonic plane-wave

$$\tilde{v}_i(x,y,t) = e^{-i\omega t} v_i(x,y) := e^{-i\omega t + i(\alpha x - \beta y)}$$

is incident on an impenetrable, sound-soft, d-periodic scattering surface shaped by $y = g(x)$. It is known [13,14] that the (reduced) scattered field $v = v(x,y)$ satisfies the following Helmholtz problem:

$$\Delta v + k^2 v = 0 \quad y > g(x), \tag{1a}$$
$$v(x,g(x)) = -v_i(x,g(x)) =: \xi(x), \tag{1b}$$
$$\text{OWC}\{v\} = 0, \tag{1c}$$

where $k^2 = \alpha^2 + \beta^2$ and v is quasi-periodic in x

$$v(x+d,y) = e^{i\alpha d} v(x,y).$$

The final condition, (1c), is the "Outgoing Wave Condition" (OWC) which can be rendered more mathematically precise [15,12] by considering a hyperplane $y = b$ strictly *above* the highest point of the surface, i.e. $b > |g|_{L^\infty}$. We augment problem (1) in the following way:

$$\Delta v + k^2 v = 0, \quad g(x) < y < b, \tag{2a}$$
$$v(x,g(x)) = \xi(x), \tag{2b}$$
$$\partial_y v(x,b) = \partial_y V(x,b), \tag{2c}$$
$$\Delta V + k^2 V = 0, \quad y > b, \tag{2d}$$
$$v(x,b) = V(x,b), \tag{2e}$$
$$\text{OWC}\{V\} = 0. \tag{2f}$$

Solutions to (1) and (2) are identical in the sense that the v agree on $\{g(x) < y < b\}$ while $v = V$ on $y > b$. Gathering (2d)–(2f) and denoting $v(x,b)$ by the generic (quasi-periodic) Dirichlet data $\psi(x)$, we recall that $V(x,y)$ can be expressed exactly as [13]

$$V(x,y) = \sum_{p=-\infty}^{\infty} \hat{\psi}_p e^{i(\alpha_p x + \beta_p y)}, \tag{3}$$

where

$$\alpha_p = \alpha + (2\pi/d)p, \qquad \beta_p = \begin{cases} \sqrt{k^2 - \alpha_p^2}, & p \in U, \\ i\sqrt{\alpha_p^2 - k^2}, & p \notin U \end{cases}$$

and

$$U := \{p \in \mathbf{Z} | k^2 - \alpha_p^2 \geqslant 0\} \tag{4}$$

and $\hat{\psi}_p$ is the pth (generalized) Fourier coefficient of $\psi(x)$. To close the system (2a)–(2c) on the *truncated* domain $\{g(x) < y < b\}$ one simply needs, given Dirichlet data $v(x,b) = V(x,b) = \psi(x)$, to produce Neumann data $\partial_y V(x,b)$, i.e. the "Dirichlet–Neumann operator" (DNO):

$$T[\psi] := \partial_y V(x,b) = \sum_{p=-\infty}^{\infty} (i\beta_p)\hat{\psi}_p e^{i\alpha_p x} =: (i\beta_D)\psi(x). \tag{5}$$

Thus (1) can be *equivalently* stated on a *truncated* domain as [15]

$$\Delta v + k^2 v = 0, \quad g(x) < y < b, \tag{6a}$$
$$v(x, g(x)) = \xi(x), \tag{6b}$$
$$\partial_y v(x,b) - T[v(x,b)] = 0. \tag{6c}$$

3. Numerical algorithms

In this section we outline some of the most popular algorithms for the numerical simulation of (1) (or, equivalently, (6)) for the purpose of illustrating their computational complexity for scattering by *families* of rough surfaces. For the case of *homogeneous* scattering the methods of choice are integral equations (Section 3.1) and field expansions (Section 3.2) which are known for their speed (in particular a surface formulation which reduces the problem dimension by one), and high accuracy. In Section 3.6 we discuss a novel implementation of the "Transformed Field Expansions" (TFE) method [12] which takes advantage of the special form of the family of scatterers to deliver not only a robust, high-order solution, but also a much faster algorithm.

3.1. Integral equations

Among the wide array of indirect or direct integral equation (IE) formulations [14] of (1), a particularly convenient one involving the *total* field ($v_t = v + v_i$) is due to Maue [16]

$$\frac{1}{2}\zeta(r) + \int_{\Sigma} \frac{\partial G(r - r')}{\partial n(r)}\zeta(r')d\sigma(r') = \frac{\partial v_i(r)}{\partial n(r)}, \qquad r \in \Sigma := \{y = g(x)\}, \tag{7}$$

where $\zeta(r) := \partial v_t(r)/\partial n(r)$ is the surface velocity, and

$$G(r) := \frac{i}{4}H_0^{(1)}(k|r|)$$

is the Helmholtz fundamental solution in two dimensions. A popular method for discretizing Maue's IE is Nyström's method [14] in which one simply enforces (7) at a set of points $\{r_j\}(1 \leqslant j \leqslant N_x)$ and seeks as unknowns, the values $\zeta(r_j)$. To recast this as a system of (linear) equations the integration in (7) must be approximated which is, by no means, a trivial task due to the singularity present in the fundamental solution. Another complication arises for scattering surfaces due to the fact that Σ is unbounded. For a general scatterer this is a feature which must be addressed for a faithful solution, however, as we are interested in *periodic* interfaces we can make a reduction of the integral to the period cell, $[0, d]$, provided that a "periodized" fundamental solution is utilized.

All of this can, however, be accomplished in a spectrally accurate manner [17], giving rise to a *dense* linear system of N_x equations with N_x unknowns. Using a direct solver these equations can be solved in $\mathcal{O}(N_x^3)$, however, this onerous computational complexity can be avoided by using preconditioned iterative solvers which have computational complexity $\mathcal{O}(N_{iter}N_x^2)$, where N_{iter} is the number of iterations [17]. This cost can be further reduced by accelerating the matrix–vector multiplications via, e.g., the Fast Multipole Method (FMM) [18,19], resulting in an algorithm with computational complexity

$$\mathcal{O}(N_{iter}N_x \log(N_x)). \tag{8}$$

3.2. Field expansions

Another computational approach to scattering by a rough surface, (1) or (6), is the method of field expansions (FE) which is Bruno and Reitich's [20–22] generalization of Rayleigh [23] and Rice's [24] classical approach. This method is based upon the observation that, above the scattering surface, the solution of (1a) and (1c) is

$$v(x,y) = \sum_{p=-\infty}^{\infty} d_p e^{i(\alpha_p x + \beta_p y)}, \tag{9}$$

c.f. (3), while the boundary condition (1b) must be used to specify the d_p. For a *single* surface which can be described as $y = g(x) = \varepsilon f(x)$, the FE approach uses the fact that the field v, and thus the Fourier coefficients d_p, depend analytically upon ε (if f is smooth) [25,12]. Thus (1b) demands that

$$\xi(x) = v(x, \varepsilon f) = \sum_{p=-\infty}^{\infty} \left(\sum_{n=0}^{\infty} d_{p,n}\varepsilon^n \right) e^{i\alpha_p x} \exp\left(i\beta_p \varepsilon f\right) = \sum_{p=-\infty}^{\infty} \sum_{n=0}^{\infty} d_{p,n}\varepsilon^n e^{i\alpha_p x} \sum_{m=0}^{\infty} F_m(i\beta_p)^m \varepsilon^m, \tag{10}$$

where $F_m(x) := f(x)^m/m!$. Expanding the left-hand-side in a generalized Fourier series and continuing

$$\sum_{p=-\infty}^{\infty} \hat{\xi}_p e^{i\alpha_p x} = \sum_{n=0}^{\infty} \varepsilon^n \sum_{l=0}^{n} \sum_{p=-\infty}^{\infty} d_{p,l} F_{n-l}(i\beta_p)^{n-l} e^{i\alpha_p x} = \sum_{n=0}^{\infty} \varepsilon^n \sum_{l=0}^{n} \sum_{p=-\infty}^{\infty} d_{p,l} \left(\sum_{q=-\infty}^{\infty} F_{n-l,q} e^{i\alpha_q x} \right) (i\beta_p)^{n-l} e^{i\alpha_p x},$$

where $F_m(x) =: \sum_{q=-\infty}^{\infty} F_{m,q} e^{i\alpha_q x}$. Finally, writing the product of the complex exponentials as a convolution, we have

$$\sum_{p=-\infty}^{\infty} \hat{\xi}_p e^{i\alpha_p x} = \sum_{n=0}^{\infty} \varepsilon^n \sum_{p=-\infty}^{\infty} e^{i\alpha_p x} \sum_{l=0}^{n} \sum_{r=-\infty}^{\infty} F_{n-l,p-r}(i\beta_r)^{n-l} d_{r,l}.$$

Remembering that $F_{0,q} = \delta_{q,0}$ (where $\delta_{n,m}$ is the Kronecker delta function), at order $\mathcal{O}(\varepsilon^n)$ we realize the recursion

$$d_{p,n} = \delta_{n,0}\hat{\xi}_p - \sum_{l=0}^{n-1} \sum_{r=-\infty}^{\infty} F_{n-l,p-r}(i\beta_r)^{n-l} d_{r,l}, \tag{11}$$

see [20]. These FE recursions can produce highly accurate solutions of scattering returns with the cost of a surface formulation,

$$\mathcal{O}(\overline{N}^2 N_x \log(N_x)), \tag{12}$$

if $\overline{N}$ Taylor orders are kept and N_x Fourier coefficients are retained. Furthermore, this is accomplished without the complications of carefully chosen integration rules, periodized fundamental solutions, or singular kernels which are all necessary for IE formulations (see Section 3.1).

3.3. Families of gratings

In [6], the author, in collaboration with F. Reitich, devised an algorithm to stably and accurately produce traveling water waves which come in *families* parameterized by the quantity ε. This algorithm produces approximations to the traveling ocean surface shape of the form

$$\eta = \eta(x; \varepsilon) = \sum_{n=1}^{\infty} \eta_n(x)\varepsilon^n. \tag{13}$$

If acoustic radiation is incident upon such an (assumed impenetrable) surface for a fixed value of ε, the IE or FE methods outlined above can be used to compute any of a number of physically relevant scattering quantities (e.g. surface velocities, efficiencies) with cost (8) or (12), respectively. However, for a *subset* of Q members of the family of ocean waves, (13), produced by the Nicholls–Reitich algorithm $(\varepsilon_1, \ldots, \varepsilon_Q)$ this cost is clearly

$$\mathcal{O}(QN_{iter}N_x \log(N_x)), \qquad \mathcal{O}(Q\overline{N}^2 N_x \log(N_x)) \tag{14}$$

for the IE and FE methods respectively. Clearly this will be quite costly for $Q \gg 1$ and, in the next sections, we outline a new computational scheme which takes advantage of the *specific* form (13) of the family of gratings, and thus has much more favorable cost for $Q \gg 1$.

3.4. Field expansions for families of gratings

To motivate our later developments, we now propose an alternative FE method specifically designed for *families* of gratings of the form

$$g = g(x; \varepsilon) = \sum_{n=1}^{\infty} f_n(x)\varepsilon^n, \tag{15}$$

c.f. (13), which takes advantage of the fact that the f_n are known. The FE methodology leads to the analogue of (10)

$$\xi = v\left(x, \sum_{n=1}^{\infty} f_n \varepsilon^n\right) = \sum_{p=-\infty}^{\infty} \left(\sum_{n=0}^{\infty} d_{p,n}\varepsilon^n \right) e^{i\alpha_p x} \exp\left(i\beta_p \sum_{n=1}^{\infty} f_n \varepsilon^n\right) = \sum_{p=-\infty}^{\infty} \left(\sum_{n=0}^{\infty} d_{p,n}\varepsilon^n \right) e^{i\alpha_p x} \left(\prod_{n=0}^{\infty} \exp\left(i\beta_p f_n \varepsilon^n\right) \right).$$

While the right-hand-side is certainly the composition of two analytic functions, the Taylor coefficients are not only complicated to compute, they will be extremely expensive requiring time proportional to $\mathcal{O}(\overline{N}!)$ for the order $\overline{N}$ coefficient. However, modifying this approach slightly can deliver enormous computational savings.

3.5. Phase extraction

One means to avoid the necessity of composing the expansion for g with the exponential function (which (1b) requires), is to remove it by a clever choice of variables. One such factorization recently proved quite useful to the authors [26] in their study of low-cost algorithms for high frequency scattering. In brief, if the scattered field is expressed as

$$v(x,y) = e^{i(\alpha x - \beta y)} w(x,y)$$

then the envelope w is guaranteed, in the absence of multiple reflections, to be slowly varying as $k^2 = \alpha^2 + \beta^2 \to \infty$. As we are not considering high frequency scattering in the current research this seems irrelevant, however, the equations satisfied by the "factored," Phase Extracted, field, w, are very useful

$$\Delta w + 2i(\alpha, -\beta) \cdot \nabla w = 0, \quad g(x) < y < b, \tag{16a}$$
$$w(x, g(x)) = -1, \tag{16b}$$
$$\partial_y w(x,b) - T_0[w(x,b)] = 0, \tag{16c}$$

where [26]

$$T_0[\psi] = i(\beta_D + \beta)\psi(x)$$

and w is *periodic* in d. Notice that these Phase Extracted equations feature no exponentiation of the profile g thus avoiding the key complication of the FE approach.

As we have mentioned before, there are many computational quantities of interest that one can simulate; among the most challenging in the current configuration is the surface velocity $\partial_\nu v$, which, for later use, we now describe in detail. This surface velocity is produced by the "Dirichlet–Neumann operator" (DNO) which is defined as

$$G(g)[\xi] := \left[-\partial_y v + (\partial_x g)\partial_x v\right]_{y=g}, \tag{17}$$

and, of course, this can also be computed via the factored quantity w

$$G(g)[\xi] = e^{i(\alpha x - \beta g)} \left[-\partial_y w + (\partial_x g)\partial_x w + \{(i\alpha)(\partial_x g) + (i\beta)\}w\right]_{y=g}.$$

Noting that the DNO also contains a common "phase" factor (similar to the one removed in the definition of w), we define the Phase Extracted DNO (PEDNO)

$$H(g) := e^{i(-\alpha x + \beta g)}G(g) = \left[-\partial_y w + (\partial_x g)\partial_x w + \{(i\alpha)(\partial_x g) + (i\beta)\}w\right]_{y=g}. \tag{18}$$

We note that once H is computed it is a simple post-processing step to produce the DNO.

3.6. Transformed field expansions for families of gratings

To finally specify our new approach we apply the useful "domain flattening" change of variables [27–29,12]

$$x' = x, \quad y' = b\left(\frac{y - g(x)}{b - g(x)}\right) \tag{19}$$

(which maps the domain $\{g < y < b\}$ to $\{0 < y' < b\}$) to (16), the Phase Extracted Helmholtz problem, and consider the transformed field

$$u(x', y') := w(x', (b - g)y'/b + g).$$

This transformation maps the problem (16) to

$$\Delta' u + 2i(\alpha, -\beta) \cdot \nabla' u = F(x', y'; u, g), \quad 0 < y' < b, \tag{20a}$$
$$u(x', 0) = -1, \tag{20b}$$
$$\partial_{y'} u(x', b) - T_0[u(x', b)] = J(x'; u, g), \tag{20c}$$

where the specific forms for F and J are given in Section A (c.f. [12]); we note that these inhomogeneities are linear or quadratic in g. We can also compute the PEDNO, H, in these new coordinates

$$H(g) = -\partial_{y'} u + (i\beta)u + K \tag{21}$$

and K is also given in Section A.

We now drop the primed variables and follow the field expansions approach outlined in Section 3.4. Considering the expansion (15) as a power series in ε, we suppose that the transformed field u also can be expressed this way as

$$u = u(x, y; \varepsilon) = \sum_{n=0}^{\infty} u_n(x, y)\varepsilon^n \tag{22}$$

importantly with the *same* perturbation parameter. To find equations for the u_n we insert (15) and (22) into (20) to realize

$$\Delta u_n + 2i(\alpha, -\beta) \cdot \nabla u_n = F_n(x, y), \quad 0 < y < b, \tag{23a}$$
$$u_n(x, 0) = -\delta_{n,0}, \tag{23b}$$
$$\partial_y u_n(x, b) - T_0[u_n(x, b)] = J_n(x), \tag{23c}$$

where the F_n and J_n are listed in Section A. The surface velocity can also be computed in this way via the PEDNO

$$H[\xi] = \sum_{n=0}^{\infty} H_n[\xi] \varepsilon^n, \tag{24}$$

where

$$H_n[\xi] = -\partial_y u_n(x, 0) + (i\beta) u_n(x, 0) + K_n(x) \tag{25}$$

and the K_n are given in Section A.

For a complete accounting of the computational cost of this "Transformed Field Expansions" (TFE) approach for families of gratings, we must remember that the change of variables introduces the inhomogeneous functions F and J into (20) necessitating a discretization of the y-direction [11,12]. However, since the "Artificial Boundary" at $y = b$ can be chosen quite close to the surface of the scatterer [12], and since we may utilize a *spectral* discretization [30,31,12], e.g. with Chebyshev polynomials, the number of unknowns N_y in the y-direction can be chosen quite small (e.g., 16 or 32). With this in mind, for a *single* scattering surface (i.e. $f_2 \equiv f_3 \equiv \cdots \equiv 0$) the cost of this algorithm is [12]:

$$\mathcal{O}(\overline{N}^2 N_x \log(N_x) N_y \log(N_y)),$$

which does *not* compare favorably with the computational complexity of the IE or FE algorithms, (8) and (12). However, we note that the computational complexity is the *same* if $f_n \neq 0$ (accommodating a general analytic family of solutions), and that once the u_n are known, any particular surface scattering quantity (e.g., the surface velocity) can be obtained by summation in time $\mathcal{O}(\overline{N} N_x)$. Thus, the total cost for a *family* of scatterers is

$$\mathcal{O}(\overline{N}^2 N_x \log(N_x) N_y \log(N_y) + Q\overline{N} N_x), \tag{26}$$

which is less than (14) as soon as

$$Q > N_y \log(N_y) \max\left\{ 1, \frac{\overline{N}^2}{N_{iter}} \right\}.$$

Now, typically $Q \gg N_y \log(N_y)$ for even a moderate sampling of the family. Furthermore, for smooth profiles the analyticity of the field guarantees that $\overline{N}$ can be chosen very small (e.g., four or six) so that our new approach becomes competitive for quite small values of Q.

3.7. Analyticity

Before proceeding to the specification of our numerical algorithm, we note that the recursions (23) can be used to show the strong convergence of the series (22). This, in turn, can be used to show the analyticity of other quantities of interest like the surface velocity (i.e. the strong convergence of the series (24)). We accomplish all of this using the framework built by the author in his collaborations with Reitich [29,32,12], Hu [33,34], Taber [35], and Fazioli [36].

For these results one needs two well-known, but by no means trivial, results: The algebra properties of Sobolev spaces, and existence and regularity results for elliptic partial differential equations. For the first we can use the following result [37,32], which features the following x-periodic Sobolev spaces:

$$H^s_{per}([0, d]) := \{f \in H^s([0, d]) | f(x + d) = f(x)\},$$
$$H^s_{per}([0, d] \times [0, b]) := \{u \in H^s([0, d] \times [0, b]) | u(x + d, y) = u(x, y)\}.$$

Lemma 1. *For any integer $s > 1/2$, if $f \in H^s_{per}([0, d])$ and $u \in H^s_{per}([0, d] \times [0, b])$, then*

$$\|fu\|_{H^s} \leqslant M \|f\|_{H^s} \|u\|_{H^s},$$

where M is a constant depending only on s.

For the second we can use the well-known "Elliptic Estimate" [38,39].

Lemma 2. *For any integer $s \geqslant 0$ there exists a constant C_e such that for any $F \in H^s_{per}([0, d] \times [0, b]), \xi \in H^{s+3/2}_{per}([0, d])$, and $J \in H^{s+1/2}_{per}([0, d])$ the solution U of*

$$\Delta U(x,y) = F(x,y), \quad (x,y) \in \{[0,d] \times [0,b]\},$$
$$U(x,0) = \xi(x),$$
$$\partial_y U(x,b) - T_0 U(x,b) = J(x),$$
$$U(x+d,y) = U(x,y)$$

satisfies

$$\|U\|_{H^{s+2}} \leqslant C_e \big\{ \|F\|_{H^s} + \|\xi\|_{H^{s+3/2}} + \|J\|_{H^{s+1/2}} \big\}.$$

We are now in a position to recursively estimate the $\{u_n\}$ in (22).

Lemma 3. *Let $s > 1/2$ be an integer and suppose that the $\{f_n\}$ in (15) satisfy*

$$\|f_n\|_{H^{s+2}} \leqslant C \frac{B^n}{(n+1)^2}, \quad \forall n.$$

Assume that

$$\|u_n\|_{H^{s+2}} \leqslant K \frac{D^n}{(n+1)^2}, \quad n < N,$$

then there exists a constant K_1 such that

$$\|F_N\|_{H^s} \leqslant KK_1 \left\{ B^2 \frac{D^{N-2}}{(N+1)^2} + B \frac{D^{N-1}}{(N+1)^2} \right\},$$

$$\|J_N\|_{H^s} \leqslant KK_1 \left\{ B^2 \frac{D^{N-2}}{(N+1)^2} + B \frac{D^{N-1}}{(N+1)^2} \right\},$$

if $B < D$.

Proof. In the interest of brevity we focus upon one particular term in F_N

$$Z_N(x,y) := \partial_y \left\{ \frac{(b-y)^2}{b^2} \sum_{m=2}^{N} \sum_{l=1}^{m-1} (\partial_x f_l)(\partial_x f_{m-l}) \partial_y u_{N-m} \right\},$$

which appears in (29). Using Lemma 1 we find that

$$\|Z_N\|_{H^s} \leqslant \left\| \frac{(b-y)^2}{b^2} \sum_{m=2}^{N} \sum_{l=1}^{m-1} (\partial_x f_l)(\partial_x f_{m-l}) \partial_y u_{N-m} \right\|_{H^{s+1}} \leqslant \frac{Y^2}{b^2} \sum_{m=2}^{N} \sum_{l=1}^{m-1} M^2 \|f_l\|_{H^{s+2}} \|f_{m-l}\|_{H^{s+2}} \|u_{N-m}\|_{H^{s+2}}$$

$$\leqslant \frac{Y^2 M^2}{b^2} \sum_{m=2}^{N} \sum_{l=1}^{m-1} C \frac{B^l}{(l+1)^2} C \frac{B^{m-l}}{(m-l+1)^2} K \frac{D^{N-m}}{(N-m+1)^2}$$

$$\leqslant K \frac{Y^2 M^2 C^2}{b^2} B^2 \frac{D^{N-2}}{(N+1)^2} \sum_{m=2}^{N} \sum_{l=1}^{m-1} \frac{(N+1)^2}{(l+1)^2 (m-l+1)^2 (N-m+1)^2} \leqslant K \frac{Y^2 M^2 C^2}{b^2} B^2 \frac{D^{N-2}}{(N+1)^2} S,$$

where $Y = M\|b-y\|_{H^{s+1}}$ and S is a finite constant that has often arisen in our previous work on analyticity with respect to boundary variations, e.g. [32,10],

$$S := \sum_{m=2}^{N} \sum_{l=1}^{m-1} \frac{(N+1)^2}{(l+1)^2 (m-l+1)^2 (N-m+1)^2} < \infty. \quad \square$$

We are now in a position to estimate the $\{u_n\}$ in such a way as to conclude analyticity of the (factored) scattered field.

Theorem 4. *Given an integer $s > 1/2$, if the $\{f_n\}$ in (15) satisfy*

$$\|f_n\|_{H^{s+2}} \leqslant C \frac{B^n}{(n+1)^2}, \quad \forall n$$

then the series (22) converges strongly. In other words, there exist constants $D, K > 0$ such that

$$\|u_n\|_{H^{s+2}} \leqslant K \frac{D^n}{(n+1)^2}, \quad \forall n \tag{27}$$

for any

$$D \geqslant \max \left\{ 1, 4C_e K_1, 2\sqrt{C_e K_1} \right\} B.$$

Proof. We work by induction on the perturbation order n. At order zero (23) is particularly simple as only the (negative unit) Dirichlet data remains on the right-hand-side so that Lemma 2 delivers

$$\|u_0\|_{H^{s+2}} \leqslant C_e \| - 1\|_{H^{s+1/2}} =: K,$$

which now defines K. We now assume the estimate (27) for all $n < N$ and examine u_N. Again, we utilize Lemma 2 which gives

$$\|u_N\|_{H^{s+2}} \leqslant C_e \{ \|F_N\|_{H^s} + \|J_N\|_{H^{s+3/2}} \}.$$

We now use Lemma 3 to demonstrate that

$$\|u_N\|_{H^{s+2}} \leqslant C_e 2KK_1 \left\{ B \frac{D^{N-1}}{(N+1)^2} + B^2 \frac{D^{N-2}}{(N+1)^2} \right\}.$$

We are finished provided that

$$D \geqslant \max \left\{ 4C_e K_1, 2\sqrt{C_e K_1} \right\} B. \qquad \square$$

Remark 5. To close this section, we note that the results of the authors in [10] provide the proper estimates on the $\{\eta_n(x)\}$ in the expansion of the surface of a traveling water wave, $\eta(x)$, in order to satisfy the hypotheses of Theorem 4. In fact, this work also demonstrates the *spatial* analyticity of the $\{\eta_n(x)\}$ as well which, though not used explicitly here, of course enables the spectral convergence of the numerical method we advocate below.

4. Numerical results

We now describe a numerical implementation of the recursions (23), producing approximations to the quantities $\{u_n\}$, which can then be used to simulate any near-field, far-field, or volumetric quantity of interest. To verify the accuracy of our implementation, in Section 4.1 we compare approximations generated with our new method to solutions given by the rigorously tested single-profile "Transformed Field Expansions" (TFE) approach outlined in [12]. Having accomplished this we study, in Section 4.2, the evolution of scattering efficiencies (a far-field quantity) as the height of a traveling ocean interface is increased. These calculations display results for hundreds or even thousands of different wave interfaces, a task that would have required extensive computational resources for standard methods, but were rapidly simulated using our new approach.

4.1. Verification

The numerical scheme is a Fourier(collocation)/Chebyshev(tau)/Taylor algorithm [30,31,11,6] applied to the system of Eq. (23). This amounts to approximating the factored field $u(x,y)$ by

Table 1
Relative error, measured in the L^∞ norm, of our new algorithm as compared with single-profile TFE [12] simulation ($N_x = 256, N_y = 64$, and $N = 30$) for frequency $(\alpha, \beta) = (1, 1)$. The base traveling wave was selected with parameters $\varepsilon = 0.1$ and $N_x = 256$. The numerical parameters for the new algorithm are $b = 1/2$ ($b = 1/10$ for $h = 1/2$), $N_x = 256, N_y = 64$, and $N = 30$.

N	$h = \infty$	$h = 2$	$h = 1$	$h = 1/2$
0	0.00115	0.00115	0.00115	0.00120
2	3.21×10^{-6}	3.81×10^{-6}	1.50×10^{-5}	0.00667
4	4.90×10^{-11}	6.44×10^{-11}	4.27×10^{-10}	3.82×10^{-7}
6	1.87×10^{-12}	1.86×10^{-12}	6.34×10^{-12}	2.97×10^{-8}
8	1.86×10^{-12}	1.86×10^{-12}	1.85×10^{-12}	2.91×10^{-11}
10	1.86×10^{-12}	1.86×10^{-12}	1.85×10^{-12}	4.55×10^{-12}

Table 2
Energy defect, E_d (c.f. (28)), at ε_{max} for four ocean depths ($h = \infty, 2, 1, 1/2$) and two scattering frequencies $((\alpha, \beta) = (1, 1), (10, 10))$. The ocean profile is 2π-periodic and the numerical parameters are $N_x = 256, N_y = 64$, and $N = 30$.

h	$(\alpha, \beta) = (1, 1)$		$(\alpha, \beta) = (10, 10)$	
	ε_{max}	E_d	ε_{max}	E_d
∞	0.43	1.17172×10^{-6}	0.30	1.11475×10^{-6}
2	0.39	2.22842×10^{-6}	0.29	1.45588×10^{-6}
1	0.29	9.70534×10^{-7}	0.21	1.38667×10^{-6}
1/2	0.11	1.15551×10^{-6}	0.08	4.82503×10^{-7}

$$u^{(N,N_x,N_y)}(x,y,\varepsilon) := \sum_{n=0}^{N} \sum_{p=-N_x/2}^{N_x/2-1} \sum_{l=0}^{N_y} \hat{u}_n^{p,l} T_l\left(\frac{2y-b}{b}\right) e^{ipx} \varepsilon^n,$$

where T_l is the lth Chebyshev polynomial. We determine the $\hat{u}_n^{p,l}$ from (23), and the Fourier collocation (x variable) and Chebyshev tau (y variable) methods. Another consideration in this approximation is the summation in n of the Taylor orders ε^n. The direct approach, simply summing the Taylor series "as is," works very well for ε *well* within the disk of analyticity of the series (22). Of course other summation techniques are available such as Padé approximation which amounts to an analytic continuation of (22). The enhanced capabilities of Padé summation are well known [40] and have been utilized with much success by the author in previous work [11,12,6]; for this reason we use this technique for all computations.

Our method also depends on the faithful computation of the terms in the Taylor series of the traveling wave, $\eta_n(x)$ (c.f. (13)), which we perform using the stable, high-order TFE method developed in [6]. In the experiments of this section we have set $b = 1/2$ ($b = 1/10$ for $h = 1/2$), $N = 30$, $N_x = 256$, and $N_y = 64$ for the computation of both the traveling waveform η and the scattered field u.

In this section we verify the accuracy of our new scheme by computing the surface velocity, G (see (17)), via H (see (18)), and comparing it with a highly accurate (and previously verified) approximation by the single-profile TFE recursions [12]. For our new method we compute an approximation
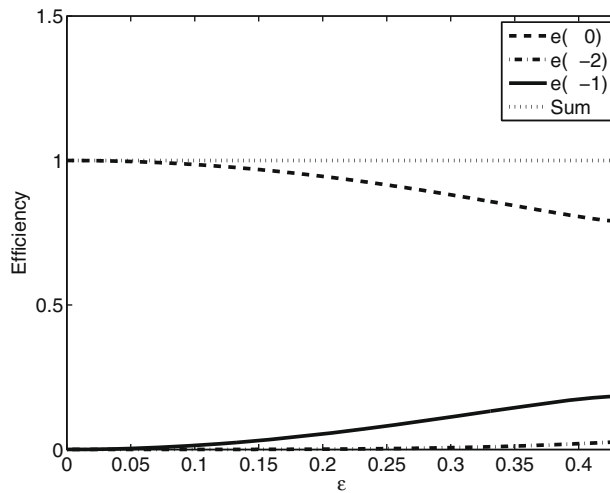

Fig. 1. Plot of the efficiencies $e_p(\varepsilon)$ for the propagating modes, $p \in U$, versus ε for an ocean of depth $h = \infty$ and radiation frequency $(\alpha, \beta) = (1, 1)$. The traveling ocean waves are non-dimensionalized to be 2π-periodic and the numerical parameters are $N_x = 256, N_y = 64$, and $N = 30$.
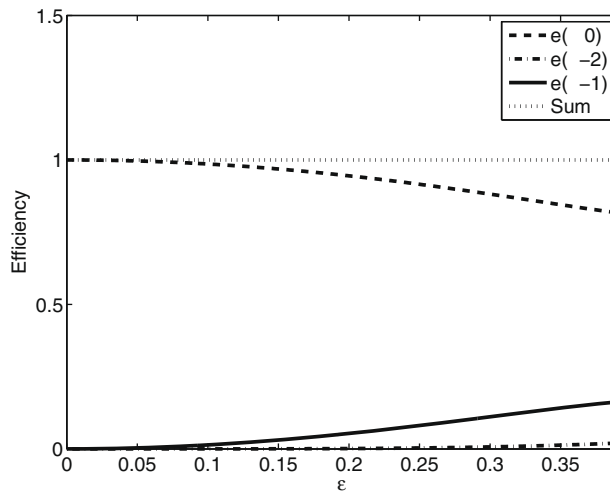

Fig. 2. Plot of the efficiencies $e_p(\varepsilon)$ for the propagating modes, $p \in U$, versus ε for an ocean of depth $h = 2$ and radiation frequency $(\alpha, \beta) = (1, 1)$. The traveling ocean waves are non-dimensionalized to be 2π-periodic and the numerical parameters are $N_x = 256, N_y = 64$, and $N = 30$.

$$H^{(N,N_x)}(x,\varepsilon) := \sum_{n=0}^{N} \sum_{p=-N_x/2}^{N_x/2-1} \widehat{H}_n^p e^{ipx} \varepsilon^n$$

using (24) and (25), which we then compare, for increasing values of N, to a single-profile TFE simulation ($N_x = 256, N_y = 64, N = 30$) [12].

We present in Table 1 the results of this convergence study for $(\alpha, \beta) = (1, 1)$, with a 2π-periodic ocean surface, ($\varepsilon = 0.01$ in (13)) on ocean depths $h = \infty, 2, 1, 1/2$. We note the precipitous convergence of our new numerical scheme to the independently obtained TFE results. Not only do they appear to be spectrally convergent, but also the "best error" (limited only by the vertical resolution) of 10^{-12} is typically realized with only 6 perturbation orders. The only exception is the much more nonlinear profile specified by $\varepsilon = 0.01$ in the shallowest depth $h = 1/2$ (which also features a slight "worsening" of the error from $N = 0$ to $N = 2$ due to the sometimes erratic behavior of Padé summation for particular values of n).

4.2. Evolution of efficiencies

Having demonstrated the accuracy of our new method, we now utilize it to study the evolution of a common far-field quantity of interest, the scattering efficiencies. Recall from (9) that the scattered field *away* from the grating surface can be represented as
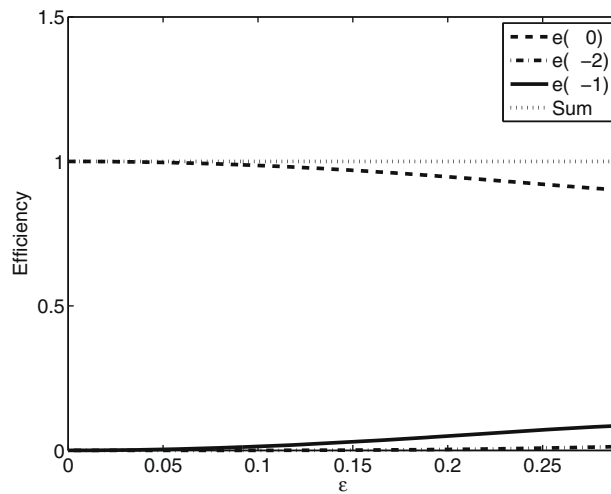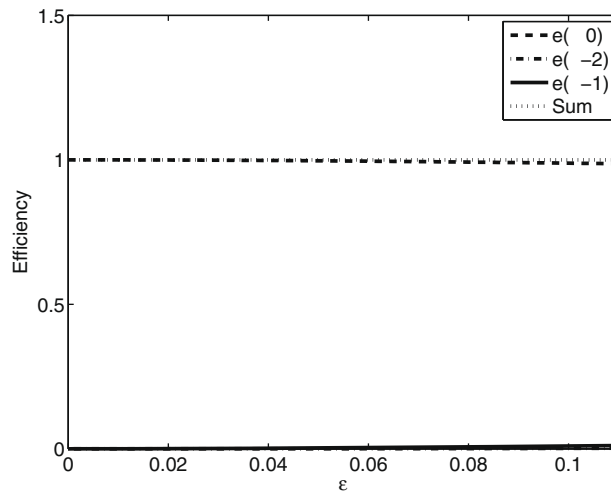

Fig. 3. Plot of the efficiencies $e_p(\varepsilon)$ for the propagating modes, $p \in U$, versus ε for an ocean of depth $h = 1$ and radiation frequency $(\alpha, \beta) = (1, 1)$. The traveling ocean waves are non-dimensionalized to be 2π-periodic and the numerical parameters are $N_x = 256, N_y = 64$, and $N = 30$.

Fig. 4. Plot of the efficiencies $e_p(\varepsilon)$ for the propagating modes, $p \in U$, versus ε for an ocean of depth $h = 1/2$ and radiation frequency $(\alpha, \beta) = (1, 1)$. The traveling ocean waves are non-dimensionalized to be 2π-periodic and the numerical parameters are $N_x = 256, N_y = 64$, and $N = 30$.

$$v(x,y) = \sum_{p=-\infty}^{\infty} d_p e^{i(\alpha_p x + \beta_p y)},$$

where the d_p are known as the "Rayleigh amplitudes." In terms of these, the efficiencies are defined as

$$e_p := \frac{\beta_p}{\beta} |d_p|^2,$$

[13] and conservation of energy implies that

$$\sum_{p \in U} |e_p|^2 = 1,$$

where we recall, c.f. (4), that U is the set of propagating waves. The efficiency gives a measure of "energy" in each mode which scatters from the grating surface, while the conservation of energy principle highlights the fact that the propagating modes make a contribution in the far-field while the decaying (evanescent, $p \notin U$) modes make a vanishingly small one.

In this section we investigate the evolution of the efficiencies $e_p = e_p(\varepsilon)$ for $p \in U$ for the four ocean depths simulated above ($h = \infty, 2, 1, 1/2$) and two rather low-frequency configurations $(\alpha, \beta) = (1, 1), (10, 10)$. These efficiencies are followed as ε is increased from zero to a maximum value where the "energy defect":
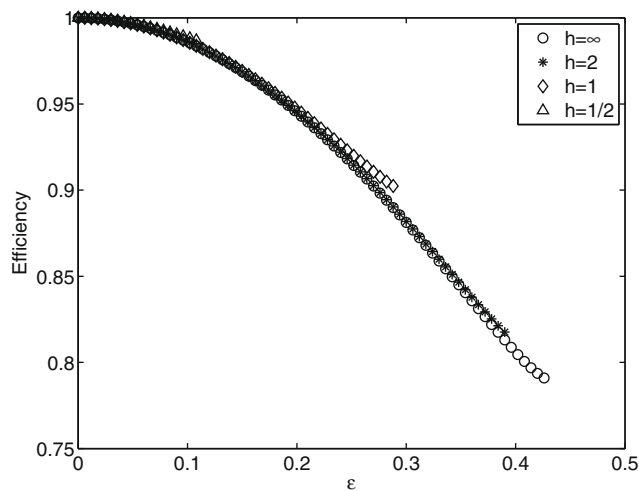

Fig. 5. Plot of efficiency $e_0(\varepsilon)$ versus ε for 2π-periodic traveling ocean waves of depths $h = \infty, 2, 1, 1/2$ and radiation frequency $(\alpha, \beta) = (1, 1)$. The numerical parameters are $N_x = 256, N_y = 64$, and $N = 30$.
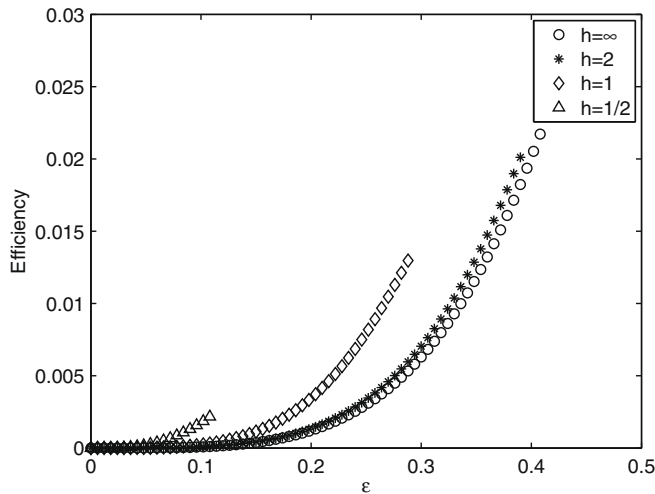

Fig. 6. Plot of efficiency $e_{-2}(\varepsilon)$ versus ε for 2π-periodic traveling ocean waves of depths $h = \infty, 2, 1, 1/2$ and radiation frequency $(\alpha, \beta) = (1, 1)$. The numerical parameters are $N_x = 256, N_y = 64$, and $N = 30$.

$$E_d := 1 - \sum_{p \in U} |e_p|^2 \qquad (28)$$

reaches a minimum tolerance (approximately 10^{-6}, see Table 2).

In Figs. 1–4 we display results of the efficiencies $e_p \in U$ evolving as a function of ε for the four ocean depths $h = \infty, 2, 1, 1/2$ in the case $(\alpha, \beta) = (1, 1)$. To create these figures our new method was used to compute the terms $u_n(x, y)$ in the expansion (22) from the recursions (23) with $N_x = 256$, $N_y = 64$, and $N = 30$. These were then sampled at the transparent boundary, $y = b$, and summed at equally spaced values of ε_j between zero and ε_{max} (listed in Table 2). The spacing was set, quite arbitrarily, at $\Delta\varepsilon = 0.001$, but any other value could have been used at very little added expense (compared to that of computing the u_n). We remark that, in this case,

$$\beta_p^2 = k^2 - \alpha_p^2 = 2 - (p+1)^2,$$

so that the set $U = \{-2, -1, 0\}$ and we follow three efficiencies. We see in all four cases that $e_0(0) = 1$ and decreases from this value as ε is increased, while $e_{-1}(0) = e_{-2}(0) = 0$ and each increase as ε increases.

To make our observations more precise we display in Fig. 5 a plot of $e_0(\varepsilon)$ for all four depths ($h = \infty, 2, 1, 1/2$) to compare their evolution as ε is varied. Here e_0 is indistinguishable for values of ε up to the largest permitted for $h = 1/2$; beyond this the remaining three curves are very close until the computation for $h = 1$ fails. Again, the final two curves are nearly insep-
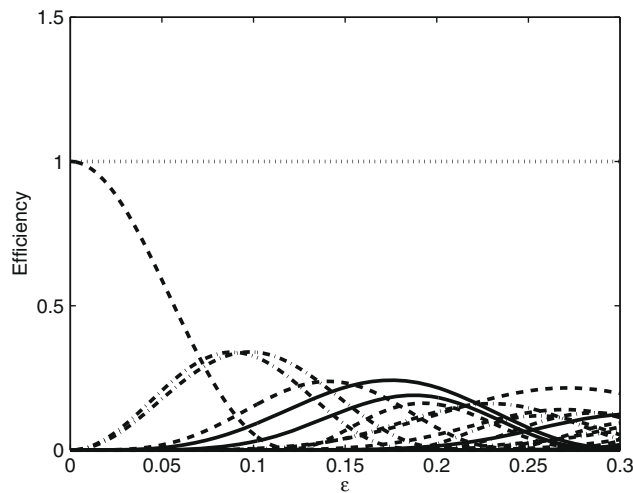

Fig. 7. Plot of the efficiencies $e_p(\varepsilon)$ for the propagating modes, $p \in U$, versus ε for an ocean of depth $h = \infty$ and radiation frequency $(\alpha, \beta) = (10, 10)$. The traveling ocean waves are non-dimensionalized to be 2π-periodic and the numerical parameters are $N_x = 256, N_y = 64$, and $N = 30$.
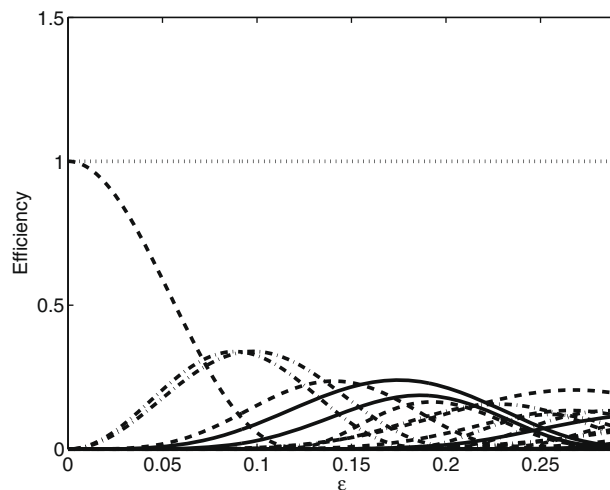

Fig. 8. Plot of the efficiencies $e_p(\varepsilon)$ for the propagating modes, $p \in U$, versus ε for an ocean of depth $h = 2$ and radiation frequency $(\alpha, \beta) = (10, 10)$. The traveling ocean waves are non-dimensionalized to be 2π-periodic and the numerical parameters are $N_x = 256, N_y = 64$, and $N = 30$.

arable until the $h = 2$ calculations diverges, while the $h = \infty$ calculation continues a little longer. In Fig. 6 we repeat this experiment for the efficiency $e_{-2}(\varepsilon)$. In this plot it is much easier to distinguish the four depths even before the divergence of each computation. This result suggests that a carefully chosen efficiency (whose evolution is markedly different for different depths) could perhaps be used as a signature for the depth of the ocean upon which a given traveling wave evolves. However, we leave such speculation for future work.

We now revisit the calculations above in the higher frequency case $(\alpha, \beta) = (10, 10)$. Here, the numerical procedure is nearly identical save that now

$$\beta_p^2 = k^2 - \alpha_p^2 = 200 - (p + 10)^2$$

and $U = \{-24, \ldots, -1, 0, 1, \ldots, 4\}$ so that 29 efficiencies are calculated. In Figs. 7–10 we follow the full spectrum of propagating efficiencies in each of the cases $h = \infty, 2, 1, 1/2$ as ε is varied. Here the pictures are much more cluttered as there are so many efficiencies to follow, so we have, once again, focused our attention on two efficiencies, e_0 and e_1, for all four depths in Figs. 11 & 12 respectively. Here, we can see that the difference in the evolution of the principal efficiency, e_0, is quite small among the four depths though it is more pronounced than in the lower frequency case $(\alpha, \beta) = (1, 1)$. We do, however, point out the non-monotone nature of the evolution of this efficiency which does help to distinguish amongst the four depths. The efficiency e_1 has a similar character to that observed for e_0 save that it begins at zero for $\varepsilon = 0$. Again, the differences among
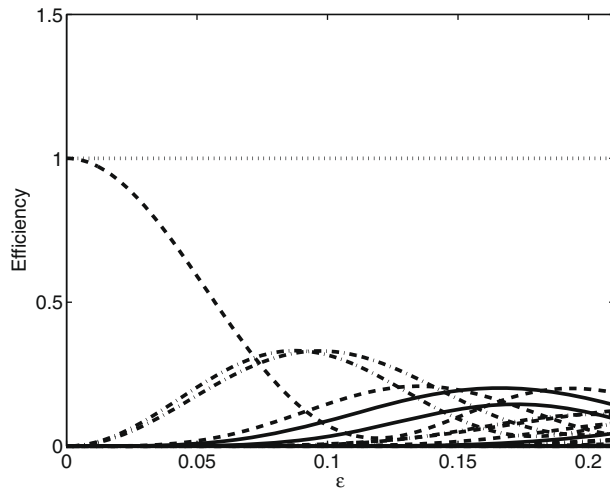

Fig. 9. Plot of the efficiencies $e_p(\varepsilon)$ for the propagating modes, $p \in U$, versus ε for an ocean of depth $h = 1$ and radiation frequency $(\alpha, \beta) = (10, 10)$. The traveling ocean waves are non-dimensionalized to be 2π-periodic and the numerical parameters are $N_x = 256, N_y = 64$, and $N = 30$.
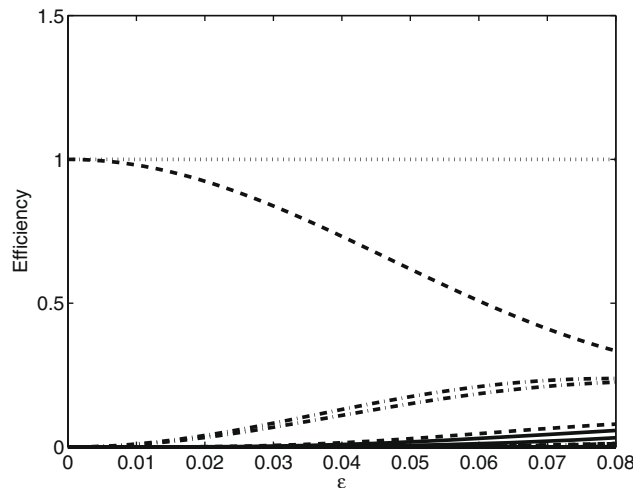

Fig. 10. Plot of the efficiencies $e_p(\varepsilon)$ for the propagating modes, $p \in U$, versus ε for an ocean of depth $h = 1/2$ and radiation frequency $(\alpha, \beta) = (10, 10)$. The traveling ocean waves are non-dimensionalized to be 2π-periodic and the numerical parameters are $N_x = 256, N_y = 64$, and $N = 30$.
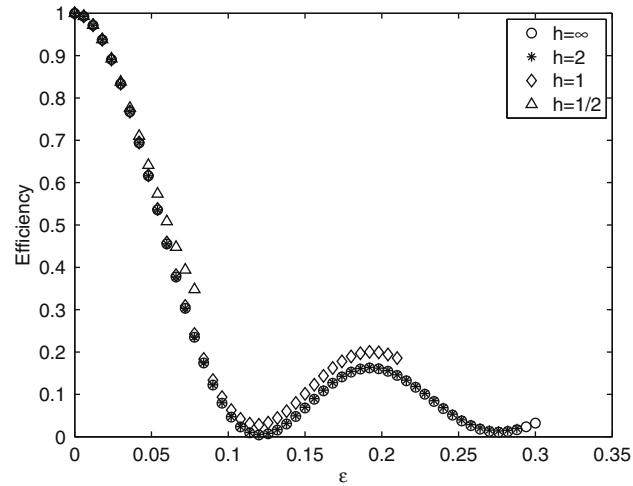
Fig. 11. Plot of efficiency $e_0(\varepsilon)$ versus ε for 2π-periodic traveling ocean waves of depths $h = \infty, 2, 1, 1/2$ and radiation frequency $(\alpha, \beta) = (10, 10)$. The numerical parameters are $N_x = 256, N_y = 64$, and $N = 30$.
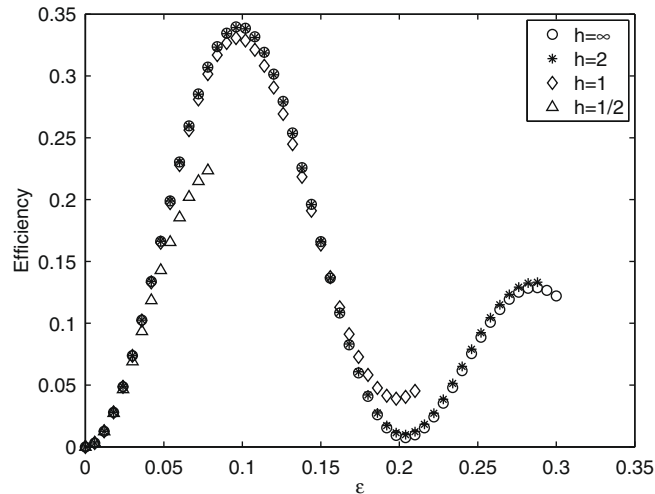

Fig. 12. Plot of efficiency $e_1(\varepsilon)$ versus ε for 2π-periodic traveling ocean waves of depths $h = \infty, 2, 1, 1/2$ and radiation frequency $(\alpha, \beta) = (10, 10)$. The numerical parameters are $N_x = 256, N_y = 64$, and $N = 30$.

the different depths are a little easier to distinguish in this "secondary" efficiency and thus may be slightly more useful as a depth diagnostic in an experimental situation.

5. Conclusion

In this paper we have developed a new Boundary Perturbation method (closely related to the method of "Transformed Field Expansions," [12]) for the rapid computation of scattering returns by a *family* of rough surfaces. The method is not only stable and high-order, but its computational complexity is substantially smaller than the current state-of-the-art solvers when applied to even a moderate sampling of the family. This is due to the fact that our new method is specially designed to have cost effectively independent of the number of family members that we sample. Using the well-known family of traveling water waves as our scattering surfaces, we not only verified the accuracy of our scheme, but we also studied the evolution of the scattering efficiencies. Such computations may be of use in the future for the remote detection and characterization of traveling waves on the surface of the ocean.

Acknowledgment

Appendix A. Specific forms for TFE inhomogeneities

In Section 3.6 we applied the change of variables (19) to the Phase Extracted Helmholtz problem (16) resulting in (20). The inhomogeneities in this equation are

$$F = \partial_{x'}F_x + \partial_{y'}F_y + F_h,$$

where

$$F_x = \frac{2}{b}g\partial_{x'}u - \frac{1}{b^2}g^2\partial_{x'}u + \frac{b-y'}{b}(\partial_{x'}g)\partial_{y'}u - \frac{b-y'}{b^2}g(\partial_{x'}g)\partial_{y'}u,$$

$$F_y = \frac{b-y'}{b}(\partial_{x'}g)\partial_{x'}u - \frac{b-y'}{b^2}g(\partial_{x'}g)\partial_{x'}u - \frac{(b-y')^2}{b^2}(\partial_{x'}g)^2\partial_{y'}u$$

and

$$F_h = -\frac{1}{b}(\partial_{x'}g)\partial_{x'}u + \frac{1}{b^2}g(\partial_{x'}g)\partial_{x'}u + \frac{b-y'}{b^2}(\partial_{x'}g)^2\partial_{y'}u - \frac{1}{b}2(i\beta)g\partial_{y'}u$$

$$- 2(i\alpha)\left\{-\frac{2}{b}g\partial_{x'}u + \frac{1}{b^2}g^2\partial_{x'}u - \frac{b-y'}{b}(\partial_{x'}g)\partial_{y'}u + \frac{b-y'}{b^2}g(\partial_{x'}g)\partial_{y'}u\right\}.$$

Additionally,

$$J = -\frac{1}{b}gT_0[u].$$

This same change of variables applied to the PEDNO, (18) gave Eq. (21) with inhomogeneity

$$K = \frac{1}{b}gH + (\partial_{x'}g)\partial_{x'}u - \frac{1}{b}g(\partial_{x'}g)\partial_{x'}u - (\partial_{x'}g)^2\partial_{y'}u + (i\alpha)(\partial_{x'}g)u - \frac{1}{b}(i\alpha)g(\partial_{x'}g)u - \frac{1}{b}(i\beta)gu.$$

Following the TFE transformation, in Section 3.6 we then followed the FE philosophy by expanding the (Phase Extracted) transformed field and PEDNO in Taylor series. The resulting inhomogeneities in (23) and (25), respectively, are

$$F_n = \partial_x F_{x,n} + \partial_y F_{y,n} + F_{h,n},$$

where

$$F_{x,n} = \frac{2}{b}\sum_{l=1}^{n}f_l\partial_x u_{n-l} - \frac{1}{b^2}\sum_{m=2}^{n}\sum_{l=1}^{m-1}f_lf_{m-l}\partial_x u_{n-m} + \frac{b-y}{b}\sum_{l=1}^{n}\partial_x f_l\partial_y u_{n-l} - \frac{b-y}{b^2}\sum_{m=2}^{n}\sum_{l=1}^{m-1}f_l\partial_x f_{m-l}\partial_y u_{n-m},$$

$$F_{y,n} = \frac{b-y}{b}\sum_{l=1}^{n}\partial_x f_l\partial_x u_{n-l} - \frac{b-y}{b^2}\sum_{m=2}^{n}\sum_{l=1}^{m-1}f_l\partial_x f_{m-l}\partial_x u_{n-m} - \frac{(b-y)^2}{b^2}\sum_{m=2}^{n}\sum_{l=1}^{m-1}\partial_x f_l\partial_x f_{m-l}\partial_y u_{n-m},\qquad(29)$$

and

$$F_{h,n} = -\frac{1}{b}\sum_{l=1}^{n}\partial_x f_l\partial_x u_{n-l} + \frac{1}{b^2}\sum_{m=2}^{n}\sum_{l=1}^{m-1}f_l\partial_x f_{m-l}\partial_x u_{n-m} + \frac{b-y}{b^2}\sum_{m=2}^{n}\sum_{l=1}^{m-1}\partial_x f_l\partial_x f_{m-l}\partial_y u_{n-m} - \frac{1}{b}2(i\beta)\sum_{l=1}^{n}f_l\partial_y u_{n-l} + 4(i\alpha)\frac{1}{b}$$

$$\times\sum_{l=1}^{n}f_l\partial_x u_{n-l} - 2(i\alpha)\frac{1}{b^2}\sum_{m=2}^{n}\sum_{l=1}^{m-1}f_lf_{m-l}\partial_x u_{n-m} + 2(i\alpha)\frac{(b-y)}{b}\sum_{l=1}^{n}\partial_x f_l\partial_y u_{n-l} - 2(i\alpha)\frac{(b-y)}{b^2}\sum_{m=2}^{n}\sum_{l=1}^{m-1}f_l\partial_x f_{m-l}\partial_y u_{n-m}.$$

We also have

$$J_n = -\frac{1}{b}\sum_{l=1}^{n}f_lT_0[u_{n-l}]$$

and

$$K_n = \frac{1}{b}\sum_{l=1}^{n}f_lH_{n-l} + \sum_{l=1}^{n}\partial_x f_l\partial_x u_{n-l} - \frac{1}{b}\sum_{m=2}^{n}\sum_{l=1}^{m-1}f_l\partial_x f_{m-l}\partial_x u_{n-m} - \sum_{m=2}^{n}\sum_{l=1}^{m-1}\partial_x f_l\partial_x f_{m-l}\partial_y u_{n-m} + (i\alpha)\sum_{l=1}^{n}\partial_x f_l u_{n-l} - \frac{1}{b}(i\alpha)\sum_{m=2}^{n}$$

$$\times\sum_{l=1}^{m-1}f_l\partial_x f_{m-l}u_{n-m} - \frac{1}{b}(i\beta)\sum_{l=1}^{n}f_lu_{n-l}.$$

References

[1] H. Lamb, Hydrodynamics, sixth ed., Cambridge University Press, Cambridge, 1993.
[2] D.J. Acheson, Elementary Fluid Dynamics, The Clarendon Press, Oxford University Press, New York, 1990.
[3] G. Stokes, On the theory of oscillatory waves, Trans. Camb. Philos. Soc. 8 (1847) 441–473.
[4] T. Levi-Civita, Détermination rigoureuse des ondes permanentes d'ampleur finie, Math. Ann. 93 (1925) 264–314.
[5] D. Struik, Détermination rigoureuse des ondes irrotationnelles périodiques dans un canal à profondeur finie, Math. Ann. 95 (1926) 595–634.
[6] D.P. Nicholls, F. Reitich, Rapid, stable, high-order computation of traveling water waves in three dimensions, Eur. J. Mech. B Fluids 25 (4) (2006) 406–424.
[7] F. Dias, C. Kharif, Nonlinear gravity and capillary-gravity waves, in: Annual Review of Fluid Mechanics, Annual Reviews, vol. 31, Palo Alto, CA, 1999, pp. 301–346.
[8] M.D. Groves, Three-dimensional travelling gravity-capillary water waves, GAMM-Mitt. 30 (1) (2007) 8–43.
[9] W. Craig, D.P. Nicholls, Traveling two and three dimensional capillary gravity water waves, SIAM J. Math. Anal. 32 (2) (2000) 323–359.
[10] D.P. Nicholls, F. Reitich, On analyticity of traveling water waves, Proc. Roy. Soc. Lond. A 461 (2057) (2005) 1283–1309.
[11] D.P. Nicholls, F. Reitich, Stability of high-order perturbative methods for the computation of Dirichlet–Neumann operators, J. Comput. Phys. 170 (1) (2001) 276–298.
[12] D.P. Nicholls, F. Reitich, Shape deformations in rough surface scattering: Improved algorithms, J. Opt. Soc. Am. A 21 (4) (2004) 606–621.
[13] R. Petit (Ed.), Electromagnetic Theory of Gratings, Springer-Verlag, Berlin, 1980.
[14] D. Colton, R. Kress, Inverse Acoustic and Electromagnetic Scattering Theory, second ed., Springer-Verlag, Berlin, 1998.
[15] D.P. Nicholls, F. Reitich, Shape deformations in rough surface scattering: cancellations, conditioning, and convergence, J. Opt. Soc. Am. A 21 (4) (2004) 590–605.
[16] A.-W. Maue, Zur Formulierung eines allgemeinen Beugungsproblems durch eine Integralgleichung, Z. Phys. 126 (1949) 601–618.
[17] F. Reitich, K. Tamma, State-of-the-art, trends, and directions in computational electromagnetics, CMES Comput. Model. Eng. Sci. 5 (4) (2004) 287–294.
[18] L. Greengard, V. Rokhlin, A fast algorithm for particle simulations, J. Comput. Phys. 73 (2) (1987) 325–348.
[19] H. Cheng, W.Y. Crutchfield, Z. Gimbutas, L.F. Greengard, J.F. Ethridge, J. Huang, V. Rokhlin, N. Yarvin, J. Zhao, A wideband fast multipole method for the Helmholtz equation in three dimensions, J. Comput. Phys. 216 (1) (2006) 300–325.
[20] O.P. Bruno, F. Reitich, Numerical solution of diffraction problems: a method of variation of boundaries, J. Opt. Soc. Am. A 10 (6) (1993) 1168–1175.
[21] O.P. Bruno, F. Reitich, Numerical solution of diffraction problems: a method of variation of boundaries. II. Finitely conducting gratings, Padé approximants, and singularities, J. Opt. Soc. Am. A 10 (11) (1993) 2307–2316.
[22] O.P. Bruno, F. Reitich, Numerical solution of diffraction problems: a method of variation of boundaries. III. Doubly periodic gratings, J. Opt. Soc. Am. A 10 (12) (1993) 2551–2562.
[23] L. Rayleigh, On the dynamical theory of gratings, Proc. Roy. Soc. London A79 (1907) 399–416.
[24] S.O. Rice, Reflection of electromagnetic waves from slightly rough surfaces, Commun. Pure Appl. Math. 4 (1951) 351–378.
[25] O.P. Bruno, F. Reitich, Solution of a boundary value problem for the Helmholtz equation via variation of the boundary into the complex domain, Proc. Roy. Soc. Edinburgh Sect. A 122 (3–4) (1992) 317–340.
[26] D.P. Nicholls, F. Reitich, Boundary perturbation methods for high-frequency acoustic scattering: Shallow periodic gratings, J. Acoust. Soc. Amer. 123 (5) (2008) 2531–2541.
[27] N.A. Phillips, A coordinate system having some special advantages for numerical forecasting, J. Atmos. Sci. 14 (2) (1957) 184–185.
[28] J. Chandezon, D. Maystre, G. Raoult, A new theoretical method for diffraction gratings and its numerical application, J. Opt. 11 (7) (1980) 235–241.
[29] D.P. Nicholls, F. Reitich, A new approach to analyticity of Dirichlet–Neumann operators, Proc. Roy. Soc. Edinburgh Sect. A 131 (6) (2001) 1411–1433.
[30] D. Gottlieb, S.A. Orszag, Numerical analysis of spectral methods: theory and applications, CBMS-NSF Regional Conference Series in Applied Mathematics, vol. 26, Society for Industrial and Applied Mathematics, Philadelphia, PA, 1977.
[31] C. Canuto, M.Y. Hussaini, A. Quarteroni, T.A. Zang, Spectral Methods in Fluid Dynamics, Springer-Verlag, New York, 1988.
[32] D.P. Nicholls, F. Reitich, Analytic continuation of Dirichlet–Neumann operators, Numer. Math. 94 (1) (2003) 107–146.
[33] B. Hu, D.P. Nicholls, Analyticity of Dirichlet–Neumann operators on Hölder and Lipschitz domains, SIAM J. Math. Anal. 37 (1) (2005) 302–320.
[34] B. Hu, D.P. Nicholls, The Domain of Analyticity of Dirichlet–Neumann Operators, submitted for publication.
[35] D.P. Nicholls, M. Taber, Joint analyticity and analytic continuation for Dirichlet–Neumann operators on doubly perturbed domains, J. Math. Fluid Mech. 10 (2) (2008) 238–271.
[36] C. Fazioli, D.P. Nicholls, Parametric analyticity of functional variations of Dirichlet–Neumann operators, Diff. Integ. Eqns. 21 (5–6) (2008) 541–574.
[37] R.A. Adams, Sobolev spaces, Pure and Applied Mathematics, vol. 65, Academic Press [A subsidiary of Harcourt Brace Jovanovich, Publishers], New York–London, 1975.
[38] L.C. Evans, Partial Differential Equations, American Mathematical Society, Providence, RI, 1998.
[39] O.A. Ladyzhenskaya, N.N. Ural'tseva, Linear and Quasilinear Elliptic Equations, Academic Press, New York, 1968.
[40] G.A. Baker Jr., P. Graves-Morris, Padé Approximants, second ed., Cambridge University Press, Cambridge, 1996.